'^{13}C Chemical Shift and ^{13}C–^{14}N Dipolar Coupling Tensors Determined by ^{13}C Rotary Resonance Solid-State NMR

Louise Odgaard,* Mads Bak,* Hans J. Jakobsen,† and Niels Chr. Nielsen*,[1]

*Laboratory for Biomolecular NMR Spectroscopy, Department of Molecular and Structural Biology, and †Instrument Centre for Solid-State NMR
Spectroscopy, Department of Chemistry, University of Aarhus, DK-8000 Aarhus C, Denmark

This work explores the utility of simple rotary resonance experiments for the determination of the magnitude and orientation of ^{13}C chemical shift tensors relative to one or more ^{13}C–^{14}N internuclear axes from ^{13}C magic-angle-spinning NMR experiments. The experiment relies on simultaneous recoupling of the anisotropic ^{13}C chemical shift and ^{13}C–^{14}N dipole–dipole coupling interactions using 2D rotary resonance NMR with RF irradiation on the ^{13}C spins only. The method is demonstrated by experiments and numerical simulations for the ^{13}C$^\alpha$ spins in powder samples of L-alanine and glycine with ^{13}C in natural abundance. To investigate the potential of the experiment for determination of relative/absolute tensor orientations and backbone dihedral angles in peptides, the influence from long-range dipolar coupling to sequential ^{14}N spins in a peptide chain (^{14}N$_i$–^{13}C$^\alpha_i$–^{14}N$_{i+1}$ and ^{14}N$_{i+1}$–^{13}C'$_i$–^{14}N$_i$ three-spin systems) as well as residual quadrupolar–dipolar coupling cross-terms is analyzed numerically.   © 2001 Academic Press

INTRODUCTION

Recently there has been an increasing interest in using anisotropic nuclear spin interactions as a probe for information about the local electronic and atomic environment of nuclear spins. In liquid-state NMR, traditionally relying on isotropic interactions and indirect effects from anisotropic interactions through relaxation, it has proven useful to induce direct influence from anisotropic chemical shift and dipolar coupling interactions by partially aligning the macromolecules in bicelle or phage solutions (*1–3*). Using known relations between the anisotropic interactions and molecular structure, these effects may provide new constraints for structure refinement. The quality of such refinement obviously depends on the anisotropic interaction parameters available. Furthermore, information about the anisotropic interaction tensors may be exploited to extract information about the structure and backbone dynamics of proteins from relaxation rates determined by solution NMR (*4*). In solid-state NMR, the same interactions may be measured directly, which has been used extensively to measure, e.g., internuclear distances and torsion angles (*5–8*). Extraction of structure information is particularly easy for the dipole–

dipole coupling interaction for which the tensor is axially symmetric and oriented along the internuclear axis. The anisotropic chemical shift parameters have typically been used based on empirical relationships between the chemical shift tensors and local structure established by solid-state NMR on related compounds. Recently, this has been supplemented by ab initio or density functional theory calculations to take more explicitly into account the specific details of the anisotropic chemical shift interaction in the determination of molecular structure (*9–12*). Such specific details include the orientation of the chemical shift tensors which may be quite sensitive, e.g., to the mutual orientation of peptide planes in biomolecules (*10*).

A variety of different solid-state NMR experiments have been proposed to provide information about anisotropic nuclear spin interactions. In addition to single-crystal NMR, which relies on the availability of a suitable-size crystal, and static powder experiments (*13*), these include magic-angle-spinning (MAS) experiments exploiting 2D exchange spectroscopy under slow-speed spinning conditions (*7*) or recoupling techniques to recover information about the anisotropic interactions under high-speed spinning conditions. The latter category includes a number of dipolar recoupling methods such as rotational resonance (*14*), rotary resonance (*15, 16*), REDOR (*17*), RFDR (*18*), HORROR (*19*), RIL (*20*), DRAWS (*21*), and C7 (*22, 23*). Furthermore, a few methods have been designed for recoupling of anisotropic chemical shift interactions either alone (*24*) or in combination with homo- and heteronuclear dipolar coupling interactions (*25*). The latter approach is particularly interesting as it may provide information about both the magnitude and the orientation of the chemical shift tensors which may add valuable constraints for structure determination. Typically, these methods have found their application for ^{13}C and/or ^{15}N isotope-labeled samples, e.g., amino acids and peptides. However, it may be relevant to extend the area of application to involve combinations with other nuclei such as ^{2}H and ^{14}N, although it is known that the quadrupolar couplings of these nuclei may complicate the performance of the experiment and the extraction of structural parameters (*26–32*).

---

[1] To whom correspondence should be addressed. E-mail: ncn@imsb.au.dk.

In this work we demonstrate that information about ^{13}C–^{14}N dipolar couplings and in particular the orientation of the ^{13}C chemical shift tensor relative to one or more ^{13}C–^{14}N internuclear axes may be obtained from a simple rotary resonance experiment with irradiation of the ^{13}C spins only. The principles of the method are demonstrated experimentally by determination of the orientation of ^{13}C$^\alpha$ chemical shift tensors relative to the ^{13}C–^{14}N internuclear axis in amino acids with all spins in natural abundance. Furthermore, using numerical simulations we explore the applicability of the experiment for determination of the orientation of ^{13}C$^\alpha$ and ^{13}C$'$ chemical shift tensors in peptides, with particular attention to the influence from remote ^{14}N spins which may complicate the extraction of orientation information but potentially also enable the extraction of absolute tensor orientation information.

THEORY

In the Zeeman interaction representation, the relevant part of the high-field truncated secular Hamiltonian for a heteronuclear spin-pair system, consisting of a spin-1/2 nucleus I and a quadrupolar nucleus S, subjected to x-phase RF irradiation on the I spin takes the form

$$H(t) = H_{\mathrm{RF}}^{(1)}(t) + H_{\mathrm{CS}}^{(1)}(t) + H_{\mathrm{D}}^{(1)}(t) + H_{\mathrm{Q}}^{(1)}(t) + H_{\mathrm{QD}}^{(2)}(t)$$

$$= \omega_{\mathrm{RF}}(t)I_x + \omega_{\mathrm{CS},0}(t)I_z + \omega_{\mathrm{D},0}(t)\frac{1}{\sqrt{6}}2I_zS_z$$

$$+ \omega_{\mathrm{Q},0}(t)\frac{1}{\sqrt{6}}(3S_z^2 - S(S+1))$$

$$- \frac{1}{2\omega_{0S}}[\omega_{\mathrm{Q},-1}(t)\omega_{\mathrm{D},1}(t) + \omega_{\mathrm{Q},1}(t)\omega_{\mathrm{D},-1}(t)]$$

$$\times I_z(3S_z^2 - S(S+1)), \qquad [1]$$

where the subscripts refer to I-spin RF irradiation (RF), I-spin chemical shift (CS), I- and S-spin dipolar coupling (D), first-order S-spin quadrupolar coupling (Q), and the second-order cross-term between S-spin quadrupolar coupling and the IS dipolar coupling (QD). $\omega_{\mathrm{RF}} = -\gamma_I B_{1I}$ and $\omega_{0S} = -\gamma_S B_0$ denote the I-spin RF field strength and S-spin Larmor frequency, respectively. For each of the nuclear spin interactions, λ, the time and orientation dependence may be expressed in terms of a Fourier series,

$$\omega_{\lambda,m'}(t) = \sum_{m=-2}^{2} \omega_{\lambda,m'}^{(m)}e^{im\omega_r t}, \qquad [2]$$

where ω_r is the spinning frequency in angular units. The Fourier coefficients are given by

$$\omega_{\lambda,m'}^{(m)} = \omega_{\mathrm{iso}}^\lambda\delta_{m=0} + \omega_{\mathrm{aniso}}^\lambda\bigg(D_{0,-m}^{(2)}(\Omega_{\mathrm{PR}}^\lambda)$$

$$- \frac{\eta^\lambda}{\sqrt{6}}[D_{-2,-m}^{(2)}(\Omega_{\mathrm{PR}}^\lambda) + D_{2,-m}^{(2)}(\Omega_{\mathrm{PR}}^\lambda)]\bigg)$$

$$\times d_{-m,m'}^{(2)}(\beta_{RL}), \qquad [3]$$

where $D^{(2)}(\Omega_{\mathrm{PR}}^\lambda) = D^{(2)}(\Omega_{\mathrm{PC}}^\lambda)D^{(2)}(\Omega_{\mathrm{CR}}^\lambda)$ is a second-rank Wigner matrix describing transformation from the principal axis frame P through a crystallite-fixed frame C to the rotor-fixed frame R. In this work C is chosen to coincide with P for the dipolar coupling interaction between the directly bonded heteronuclei. $d_{m,m'}^{(2)}(\beta_{RL})$ is an element of the reduced Wigner matrix specifying transformation from R to the laboratory frame L through the magic angle $\beta_{RL} = \cos^{-1}\sqrt{3}$. For the chemical shift interaction the isotropic and anisotropic frequency components are $\omega_{\mathrm{iso}}^{\mathrm{CS}} = \omega_{0I}\delta_{\mathrm{iso}}$ ($\omega_{0I} = -\gamma_I B_0$ is the I-spin Larmor frequency) and $\omega_{\mathrm{aniso}}^{\mathrm{CS}} = \omega_{0I}\delta_{\mathrm{aniso}}$, respectively. The isotropic chemical shift, the chemical shift anisotropy, and the asymmetry parameter are related to the principal elements of the chemical shift tensor as $\delta_{\mathrm{iso}} = \frac{1}{3}(\delta_{xx} + \delta_{yy} + \delta_{zz})$, $\delta_{\mathrm{aniso}} = \delta_{zz} - \delta_{\mathrm{iso}}$, and $\eta^{\mathrm{CS}} = (\delta_{yy} - \delta_{xx})/\delta_{\mathrm{aniso}}$, respectively ($|\delta_{zz} - \delta_{\mathrm{iso}}| \geq |\delta_{xx} - \delta_{\mathrm{iso}}| \geq |\delta_{yy} - \delta_{\mathrm{iso}}|$). For the dipolar coupling interaction, we have $\omega_{\mathrm{iso}}^{\mathrm{D}} = 0$, $\omega_{\mathrm{aniso}}^{\mathrm{D}} = \sqrt{6}\,b_{IS}$, and $\eta^{\mathrm{D}} = 0$, where the dipolar coupling constant $b_{IS}/2\pi$ is related to the internuclear distance r_{IS} according to $b_{IS} = -\gamma_I\gamma_S\mu_0\hbar/(r_{IS}^3 4\pi)$. The quadrupolar coupling interaction is characterized by $\omega_{\mathrm{iso}}^{\mathrm{Q}} = 0$, $\omega_{\mathrm{aniso}}^{\mathrm{Q}} = \sqrt{6}\,\pi C_{\mathrm{Q}}/(2S(2S-1))$ and η^{Q} where $C_{\mathrm{Q}} = e^2Qq/h$ is the quadrupolar coupling constant.

In the present study we are interested in determining the magnitude and orientation of ^{13}C chemical shift tensors relative to one or more ^{13}C–^{14}N internuclear axes in spin systems where the ^{13}C spin is dipolar coupled to at least one ^{14}N spin. In the first part of the paper we focus attention on a ^{13}C–^{14}N spin pair. Considering that even for directly bonded nuclei the ^{13}C–^{14}N dipolar coupling is relatively weak and that sample spinning is necessary to obtain high-resolution spectra, this requires exploitation of residual effects from ^{13}C–^{14}N dipolar coupling and ^{14}N quadrupolar coupling second-order cross-terms in MAS spectra (26, 27, 33) or the use of experiments which actively prevents MAS averaging of the ^{13}C–^{14}N dipolar coupling. Focusing on the dipolar coupling alone, the latter may, e.g., be accomplished using a rotational-echo experiment (29). In the present case where we additionally are interested in the ^{13}C chemical shift anisotropy, it may be more relevant to use variable-angle spinning (28) or, as discussed earlier by Bak and Nielsen (25), a simple rotary resonance experiment (15, 16) to simultaneously recouple the ^{13}C–^{14}N dipolar coupling and the ^{13}C chemical shift interactions under high-resolution MAS conditions. In its basic form the rotary resonance experiment consists of a weak ^{13}C RF pulse of duration t_1 bracketed by $(\pi/2)_y$ and $(\pi/2)_{\bar{y}}$ pulses with I_z being representative of both the initial and the detected operator (25). Relying on cross-
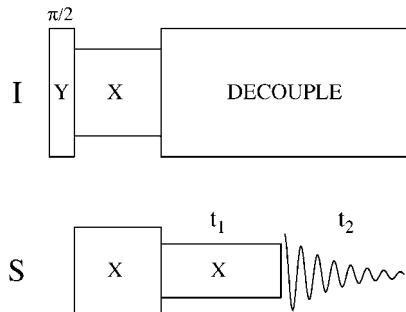
FIG. 1. Timing scheme for the 2D rotary resonance recoupling MAS experiment starting with cross-polarization from the ^{1}H spins. Simultaneous recoupling of the ^{13}C chemical shift anisotropy and the ^{13}C–^{14}N dipolar coupling in the t_1 period is achieved by on-resonance RF irradiation of the ^{13}C nuclei using a RF field strength adjusted to $\omega_{RF}/2\pi = n\omega_r/2\pi$ with $n = 1$ or 2.

polarization from the abundant ^{1}H spins and detection of transverse coherence for the ^{13}C spins, this leads to the practically relevant pulse sequence in Fig. 1 with the amplitude of the weak RF field (ω_{RF}) during t_1 adjusted to fulfill the rotary resonance condition (15, 16)

$$\omega_{RF} = n\omega_r, \qquad [4]$$

where the I-spin RF carrier frequency is on-resonance with respect to the relevant ^{13}C spins and n is a small integer different from zero. We note that $|n| = 1$ promotes recoupling of homo- and heteronuclear dipolar couplings as well as anisotropic chemical shift interactions (25), while only the two latter are recoupled for $|n| = 2$.

The recoupling effect becomes evident in the interaction frame of the pulse sequence, defined by the transformation (15, 16, 25)

$$\tilde{A} = U_{RF}^{\dagger}(t)A(t)U_{RF}(t), \qquad [5]$$

$$U_{RF}(t) = e^{-i(\pi/2)I_y}e^{-in\omega_r tI_z}, \qquad [6]$$

using the relation in Eq. [4]. In this frame we obtain

$$\tilde{H}_{CS}^{(1)} = -\frac{1}{2}\sum_{m=-2}^{2}\omega_{CS,0}^{(m)}[e^{i(m+n)\omega_r t}I^+ + e^{i(m-n)\omega_r t}I^-], \qquad [7]$$

$$\tilde{H}_{D}^{(1)} = -\frac{1}{\sqrt{6}}\sum_{m=-2}^{2}\omega_{D,0}^{(m)}[e^{i(m+n)\omega_r t}I^+ + e^{i(m-n)\omega_r t}I^-]S_z, \qquad [8]$$

$$\tilde{H}_{QD}^{(2)} = \frac{1}{4\omega_{0S}}\sum_{m,m'=-2}^{2}[\omega_{Q,-1}^{(m)}\omega_{D,1}^{(m')}e^{i(m+m'+n)\omega_r t}I^+$$
$$+ \omega_{Q,1}^{(m)}\omega_{D,-1}^{(m')}e^{i(m+m'-n)\omega_r t}I^-]$$
$$\times (3S_z^2 - S(S + 1)), \qquad [9]$$

$$\tilde{H}'^{(2)}_{QD} = -\frac{1}{2\omega_{0S}}\sum_{m,m'=-2}^{2}[\omega_{Q,-1}^{(m)}\omega_{D,1}^{(m')} + \omega_{Q,1}^{(m)}\omega_{D,-1}^{(m')}]$$
$$\times e^{i(m+m')\omega_r t}I_z(3S_z^2 - S(S + 1)), \qquad [10]$$

where the last term has been included to represent the effect of the quadrupolar–dipolar coupling cross-term under standard MAS conditions (i.e., in the t_2 detection period of the 2D experiment). The first-order average Hamiltonians taken over one rotor period,

$$\bar{\tilde{H}}_{CS}^{(1)} = -\frac{1}{2}[\omega_{CS,0}^{(-n)}I^+ + \omega_{CS,0}^{(n)}I^-] \qquad [11]$$

$$\bar{\tilde{H}}_{D}^{(1)} = -\frac{1}{\sqrt{6}}[\omega_{D,0}^{(-n)}I^+ + \omega_{D,0}^{(n)}I^-]S_z \qquad [12]$$

$$\bar{\tilde{H}}_{QD}^{(2)} = \frac{1}{4\omega_{0S}}\sum_{m=-2}^{2}[\omega_{Q,-1}^{(m)}\omega_{D,1}^{(-n-m)}I^+ + \omega_{Q,1}^{(m)}\omega_{D,-1}^{(n-m)}I^-]$$
$$\times (3S_z^2 - S(S + 1)) \qquad [13]$$

$$\bar{\tilde{H}}'^{(2)}_{QD} = -\frac{1}{2\omega_{0S}}\sum_{m=-2}^{2}[\omega_{Q,-1}^{(m)}\omega_{D,1}^{(-m)} + \omega_{Q,1}^{(m)}\omega_{D,-1}^{(-m)}]$$
$$\times I_z(3S_z^2 - S(S + 1)), \qquad [14]$$

reveal that simultaneous recoupling of the anisotropic I-spin chemical shift and the heteronuclear dipolar coupling is obtained when one of the two lowest order rotary resonance conditions in Eq. [4] is fulfilled. Furthermore, it is apparent that residual (i.e., stationary) components of the quadrupolar–dipolar coupling cross-term exist both in the case of rotary resonance (Eq. [13]) and under normal MAS (Eq. [14]) conditions, although in different forms.

To evaluate their practical influence on the NMR experiments, it is of interest to consider the magnitudes of the various terms in Eqs. [11]–[14]. For this purpose we assume $\eta^\lambda = 0$, simplifying the relevant Fourier components to

$$\omega_{\lambda,0}^{(\pm 1)} = -\frac{1}{2\sqrt{2}}\omega_{aniso}^\lambda\sin(2\beta_{PR}^\lambda)e^{\pm i\gamma_{PR}^\lambda} \qquad [15]$$

$$\omega_{\lambda,0}^{(\pm 2)} = \frac{1}{4}\omega_{aniso}^\lambda\sin^2(\beta_{PR}^\lambda)e^{\pm 2i\gamma_{PR}^\lambda} \qquad [16]$$

$$\omega_{\lambda,[\pm 1]}^{(0)} = \frac{[\pm 1]}{\sqrt{3}}\, \omega_{\text{aniso}}^{\lambda}\, \frac{3\cos^2(\beta_{\text{PR}}^{\lambda}) - 1}{2} \qquad [17]$$

$$\omega_{\lambda,[\pm 1]}^{(\pm 1)} = \frac{[\pm 1] \pm \sqrt{3}}{4\sqrt{6}}\, \omega_{\text{aniso}}^{\lambda}\sin(2\beta_{\text{PR}}^{\lambda})e^{\pm i\gamma_{\text{PR}}^{\lambda}} \qquad [18]$$

$$\omega_{\lambda,[\pm 1]}^{(\pm 2)} = \frac{[\mp 1] \pm \sqrt{3}}{4\sqrt{3}}\, \omega_{\text{aniso}}^{\lambda}\sin^2(\beta_{\text{PR}}^{\lambda})e^{\pm 2i\gamma_{\text{PR}}^{\lambda}}. \qquad [19]$$

Using these expressions it is possible to estimate the impact of the various interactions to the spin dynamics. For an $n = 1$ rotary resonance experiment the coefficients to the spin operations may be expressed as

$$\bar{\bar{H}}_{\text{CS}}^{(1)} : \frac{1}{2}\,|\omega_{\text{CS},0}^{(1)}|/2\pi \leq \frac{1}{2}\,\omega_{\text{aniso}}^{\text{CS}}/2\pi \qquad [20]$$

$$\bar{\bar{H}}_{\text{D}}^{(1)} : \frac{1}{\sqrt{6}}\,|\omega_{\text{D},0}^{(1)}|/2\pi \leq \frac{1}{2\sqrt{2}}\,b_{IS}/2\pi \qquad [21]$$

$$\bar{\bar{H}}_{\text{QD}}^{(2)} : \frac{1}{4\omega_{0S}}\,|\omega_{\text{Q},-1}^{(0)}\omega_{\text{D},1}^{(1)}|/2\pi \leq \frac{1+\sqrt{3}}{32\sqrt{2}}\,\frac{C_{Q}b_{IS}/2\pi}{\omega_{0S}/2\pi} \qquad [22]$$

$$\bar{\bar{H}}'^{(2)}_{\text{DQ}} : \frac{1}{2\omega_{0S}}\,|\omega_{\text{Q},-1}^{(0)}\omega_{\text{D},1}^{(0)}|/2\pi \leq \frac{1}{4}\,\frac{C_{Q}b_{IS}/2\pi}{\omega_{0S}/2\pi}, \qquad [23]$$

where the maximum value applies for the most influential β_{PR} crystallite angle. It should be noted that for the quadrupolar–dipolar coupling cross-terms we consider for simplicity only the dominant among several terms as given by Eqs. [13] and [14].

Taking typical values of $b_{IS}/2\pi = -650$ Hz (corresponding to a C–N distance of 1.5 Å), $C_Q = 1.2$ MHz, $\omega_{\text{aniso}}^{\text{CS}}/2\pi = 2$ kHz, and $\omega_{0S}/2\pi = 28.9$ MHz relevant for the study of ^{13}C$^{\alpha}$ carbons in amino acids (33–37) or peptides using a 400-MHz (9.4-T) NMR spectrometer, the right-hand sides of Eqs. [20] through [23] take the maximum values 1000, 230, 1.6, and 6.5 Hz, respectively. These values reveal that the dominant interactions are the anisotropic chemical shift and the heteronuclear dipolar coupling (we note that the effective dipolar coupling frequency is scaled by an additional factor of 2 because of the $I = 1$ spin part of the interaction), while the quadrupolar–dipolar coupling cross-terms largely vanish using a 9.4-T static magnetic field. This conclusion for the cross-terms, in particular under rotary resonance conditions, holds even upon scaling of these terms by an estimated factor of 3–7 originating from simultaneous interplay of about 10 recoupled components in Eqs. [13] and [14] with different orientational dependencies. Accordingly, we can safely ignore influence from the ^{14}N quadrupolar coupling interaction in the following.

EXPERIMENTAL

All spectra were recorded on a Varian Unity-INOVA 400 (9.4-T) widebore NMR spectrometer using a homebuilt 4-mm ^{1}H–X double-resonance MAS probe. To reduce effects from RF inhomogeneity each sample was restricted to a 1-mm-thick slice in the center of the 4-mm-o.d. Si_3N_4 rotor. Radiofrequency field strengths of 72.4, 35.4, and 6.0 kHz were used for the ^{1}H pulses and decoupling, ^{1}H and ^{13}C spin-lock during cross polarization, and ^{13}C rotary resonance irradiation, respectively. The spinning speed was controlled to $\omega_r/2\pi = 6000 \pm 3$ Hz. The 2D rotary resonance spectra were obtained using 120 scans for each of the 128 t_1 increments separated by $\Delta t_1 = 2\pi/(3\omega_r) = 55.6$ μs (4-s relaxation delay). The ^{13}C chemical shifts are reported in parts per million relative to external TMS. Polycrystalline powders of L-alanine and glycine were obtained from Merck and used without any further purification. Numerical simulations and iterative fitting of the $\omega_1/2\pi$ dimension of the experimental 2D rotary resonance spectra were performed on a 450-MHz Pentium III processor using the SIMPSON simulation program (38). Each simulation, using 256 to 678 α_{CR} and β_{CR} crystallite angles selected using the REPULSION scheme (39) and 3–12 γ_{CR} angles implemented using γ-COMPUTE (40), typically required 2 and 30 s of CPU time for ^{13}C–^{14}N and ^{14}N–^{13}C–^{14}N spin systems, respectively.

RESULTS AND DISCUSSION

Considering an amino acid ^{13}C$^{\alpha}$–^{14}N spin system, the simultaneous recoupling of the anisotropic ^{13}C$^{\alpha}$ chemical shift and ^{13}C$^{\alpha}$–^{14}N dipolar coupling interaction by $n = 1$ rotary resonance RF irradiation of the ^{13}C$^{\alpha}$ spin is illustrated by the numerical simulations in Fig. 2. The $\omega_1/2\pi$ projections are calculated on basis of the parameters for the ^{13}C$^{\alpha}$–^{14}N spin pair in L-alanine (*vide infra*) with Fig. 2 showing spectra for a single crystal with $\Omega_{\text{CR}} = \{0, \pi/4, 0\}$ without and with chemical shift anisotropy as well as powder spectra calculated under the same conditions. The first of these spectra (Fig. 2a) shows a regular 1:1:1 triplet with the outer peaks at $\pm(1/\sqrt{2})\,b_{IS}/2\pi$ with the present value of $b_{IS}/2\pi = -665$ Hz for the dipolar coupling constant corresponding to an internuclear distance of 1.486 Å. Upon powder averaging (Fig. 2b) this triplet transforms into a broadened 1:2:1 triplet due to the β_{CR} crystallite angle dependence on the outer peaks. Adding a typical (and dominant) value for the ^{13}C$^{\alpha}$ chemical shift anisotropy (specifically $\omega_{\text{CS}}^{\text{aniso}}/2\pi = 1978$ Hz) markedly perturbs the lineshape leading to the single-crystal and powder spectra in Figs. 2c and 2d, respectively. We note that a very similar behavior as that described here for the $n = 1$ case is obtained for $n = 2$ rotary resonance spectra (not shown) where the overall scaling factor for both anisotropic shift and dipolar coupling is reduced by a factor of $1/\sqrt{2}$. The different powder angle dependency, however, causes different lineshapes for the $n = 1$ and 2 cases.
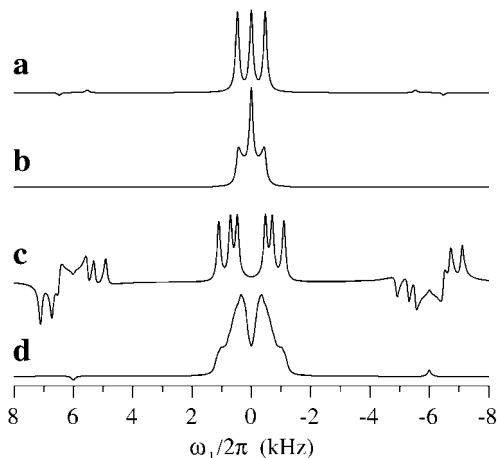
FIG. 2. $\omega_1/2\pi$ projections from ^{13}C $n = 1$ 2D rotary resonance spectra calculated using the ^{13}C$^\alpha$–^{14}N spin-pair parameters for L-alanine (parameters in Table 1) (a) for a single-crystal with $\Omega_{CR} = \{0, \pi/4, 0\}$ and $\omega_{CS}^{aniso} = 0$, (b) as (a) but for a powder, (c) as (a) but with the chemical shift anisotropy included, and (d) as (c) but for a powder. The spectra used $\omega_{RF}/2\pi = \omega_r/2\pi = 6000$ Hz, 256 t_1 values separated by $2\pi/(3\omega_r)$, and data processing with zero-filling to 8192 points and apodization using a 135-Hz Lorentzian line broadening.

a. Isolated ^{13}C–^{14}N Spin Pairs

Figures 3 to 6 give practical examples demonstrating applications of the $n = 1$ rotary resonance experiment for determination of the magnitude and orientation of the ^{13}C$^\alpha$ chemical shift tensor relative to the ^{13}C$^\alpha$–^{14}N internuclear axis from powders of amino acids with all spin isotopes in natural abundance. For the purpose of illustration we have chosen L-alanine (Figs. 3–5) and glycine (Fig. 6) for which the crystal structures have been determined using neutron diffraction (34, 35) and the anisotropic tensors for the ^{13}C$^\alpha$–^{14}N spin pairs are known a priori from single-crystal (36, 37) and MAS (25, 33) solid-state NMR. This provides an appropriate basis for evaluation of the parameters established using the rotary resonance approach for tensor determination.

From neutron diffraction it is known that L-alanine is orthorhombic with space group $P2_12_12_1$ (34). The crystal structure has four molecules in the unit cell with the shortest intra- and intermolecular C$^\alpha$–N internuclear distances being 1.486 and 4.11 Å, respectively, corresponding to dipolar coupling constants of -665 and -31 Hz. The latter dipolar coupling is sufficiently small that, to a good approximation, we can consider the intramolecular ^{13}C$^\alpha$–^{14}N spins representing an isolated two-spin system. Figure 3a shows the $\omega_1/2\pi$ projection of an experimental $n = 1$ 2D rotary resonance experiment of L-alanine recorded at 9.4 T using the pulse sequence in Fig. 1. Below the experimental spectrum we show a numerical simulation resulting from iterative fitting of the experimental spectrum and finally a spectrum representing the difference between the experimental and the simulated spectrum. The iterative fitting is based on values for the dipolar coupling constant and parameters for the magnitude of the ^{13}C$^\alpha$ chemical

shift tensor known from single-crystal NMR experiments (i.e., $b_{IS}/2\pi = -665$ Hz, $\omega_{CS}^{aniso}/2\pi = 1978$ Hz, and $\eta^{CS} = 0.44$) (36). We note that these values for the chemical shift anisotropy and asymmetry parameter may readily be confirmed with an accuracy within 100 Hz and 0.2, respectively, using a standard ^{13}C MAS experiment with $\omega_r/2\pi = 1200$ Hz in this
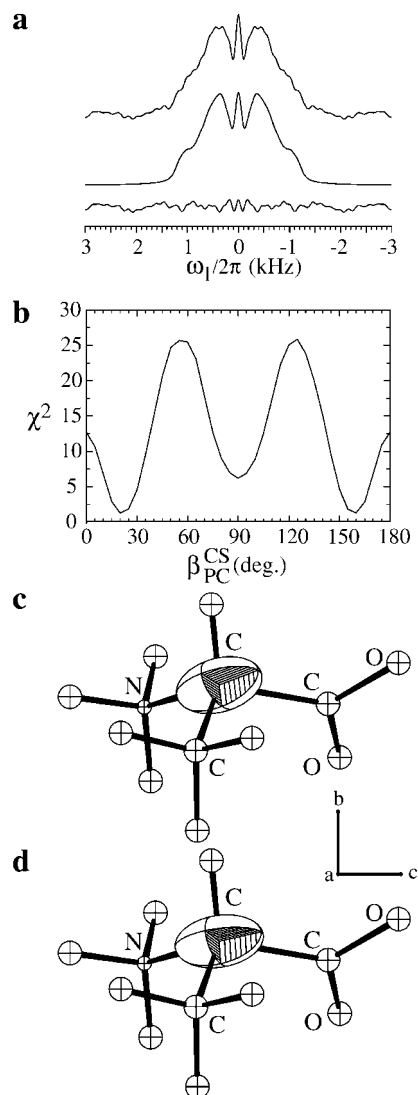

FIG. 3. (a) $\omega_1/2\pi$ projections from experimental and simulated ^{13}C $n = 1$ 2D rotary resonance ^{13}C MAS NMR spectra of ^{13}C$^\alpha$ in L-alanine along with a spectrum showing the difference between the experimental and simulated spectra. The parameters corresponding to the simulated spectrum (obtained by least-squares fitting to the experimental spectrum) are given in Table 1 and represented by the ORTEP-like plot in (c) (note that γ_{PC}^{CS} is not established from (a) and have been arbitrarily chosen to give the best visual match with (d)). The best agreement with the experimental spectrum was obtained for a RF field strength of $\omega_{RF}/2\pi = 6123$ Hz and a Lorentzian line broadening of 163 Hz. For comparison (d) includes a similar representation of the parameters determined by single-crystal NMR (36). (b) Plot of the $\chi^2 = 10^3 \sum_{i=1}^{N} (S_i^{exp} - S_i^{sim})^2/(\sum_{i=1}^{N} (S_i^{exp} + S_i^{sim})^2)$ deviation between the experimental (S_i^{exp}) and simulated (S_i^{sim}) spectra ($i = 1, 2, \ldots, N$ points upon zero-filling) as function of β_{PC}^{CS} (see text).
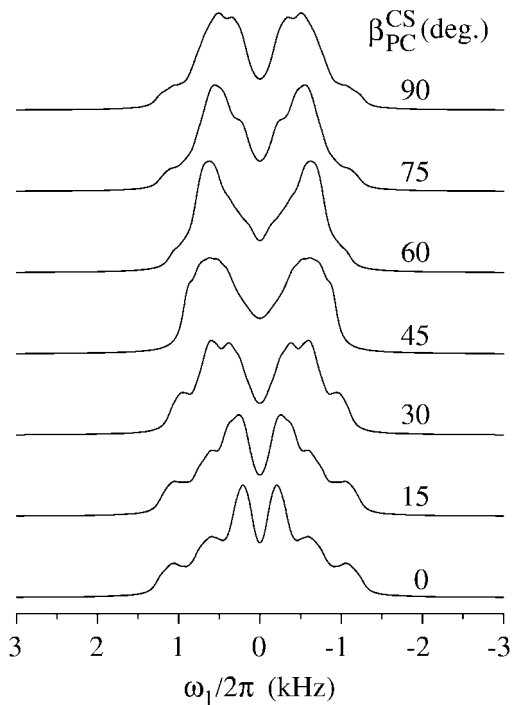
FIG. 4. $\omega_1/2\pi$ projections from ^{13}C $n = 1$ 2D rotary resonance spectra calculated using the ^{13}C$^\alpha$–^{14}N spin-pair parameters for L-alanine (cf. Table 1) except $\alpha_{PC}^{CS} = \gamma_{PC}^{CS} = 0$ and variation of β_{PC}^{CS} in steps of 15° from 0° to 90°. All spectra used $\omega_r/2\pi = \omega_{RF}/2\pi = 6000$ Hz and a Lorentzian line broadening of 135 Hz.

minima, however, are clearly distinguished by the root-mean-square deviation or χ^2 value. This aspect and the general sensitivity of the spectra toward variation in β_{PC}^{CS} are demonstrated in Fig. 3b by a χ^2 versus β_{PC}^{CS} scan through the range of β_{PC}^{CS} angles from 0 to 180° with optimization of the other variables throughout the scan. Figure 3c gives an ORTEP-like representation of the magnitude and optimum orientation of the ^{13}C$^\alpha$ chemical shift tensor in the molecular frame of L-alanine. For comparison, Fig. 3d shows the corresponding ORTEP-like representation of the ^{13}C$^\alpha$ shift tensor determined by Naito *et al.* using single-crystal NMR (*36*). It is relevant to note that the β_{PC}^{CS} value determined by rotary resonance agrees within 4° with the value determined in the single-crystal NMR study. Obviously, the sensitivity of the experiment toward variations in the orientational parameters is not only reflected in one single parameter such as χ^2. Specific details in the $\omega_1/2\pi$ lineshape may in a sensitive manner give a direct estimate of the parameters as demonstrated in Fig. 4 by $\omega_1/2\pi$ projections calculated using the same parameters as for the L-alanine spectra in Fig. 3, except $\omega_r/2\pi = \omega_{RF}/2\pi = 6000$ Hz, $\alpha_{PC}^{CS} = \gamma_{PC}^{CS} = 0$, and variation of β_{PC}^{CS} in steps of 15° from 0° to 90°. Although these spectra are not selected to match exactly the extrema of the β_{PC}^{CS} scan in Fig. 3b, it is evident that the powder lineshape critically depends on the orientational parameters. Furthermore, although not being focused on in detail in this study, the spectra obviously also display sensitivity toward the
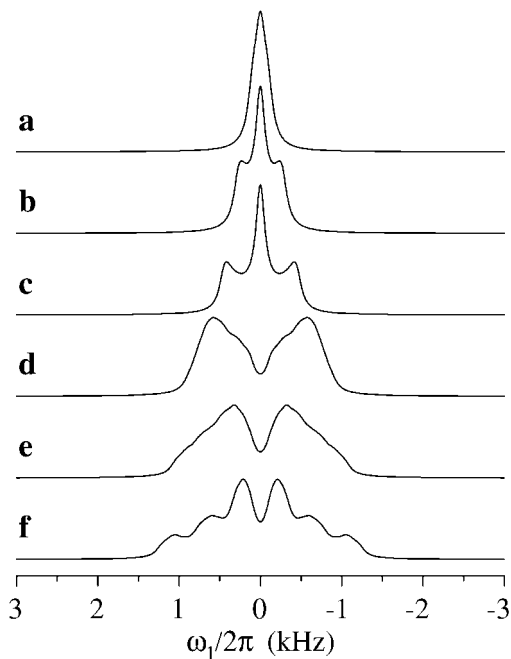
case. Thus, considering only small uncertainty in these parameters as well as a known limited variation in the one-bond ^{13}C–^{14}N dipolar coupling constant in general, the free variables in the iterative fitting were the Ω_{PC}^{CS} Euler angles describing the orientation of the chemical shift tensor relative to the C$^\alpha$–N internuclear axis along with variables describing minor variations in the RF field strength and an additional Lorentzian linebroadening. The latter takes into account minor effects from T_2 relaxation and RF inhomogeneity as well as nonresolved effects from long-range dipolar couplings and the residual quadrupolar–dipolar coupling cross terms. We note that the axial symmetry of the dipolar coupling tensor (oriented along the internuclear axis) in this two-spin case only allows us to determine two of the three Euler angles, among which the spectra are most sensitive to the β_{PC}^{CS} angle between the unique element of the ^{13}C chemical shift tensor (being the most shielded element for L-alanine) and the ^{13}C–^{14}N axis.

The best agreement between the experimental and simulated spectra of L-alanine was obtained for the ^{13}C$^\alpha$ chemical shift tensor orientation $\alpha_{PC}^{CS} = -51°$ and $\beta_{PC}^{CS} = 21.7°$ in the principal axis frame of the ^{13}C$^\alpha$–^{14}N dipolar coupling interaction (i.e., $\Omega_{PC}^{IS} = \{0, 0, 0\}$). The parameters resulting from the iterative fitting are summarized in Table 1 along with the parameters resulting from earlier NMR and neutron diffraction studies. We note that the iterative fitting leads to two different local minima, corresponding to different tensor orientations. The two

FIG. 5. $\omega_1/2\pi$ projections from ^{13}C $n = 1$ 2D rotary resonance spectra calculated using the ^{13}C$^\alpha$–^{14}N spin-pair parameters for L-alanine (cf. Table 1) except for $b_{IS}/2\pi$, which takes values of (a, d) -150 Hz ($r_{IS} = 2.44$ Å), (b, e) -400 Hz ($r_{IS} = 1.76$ Å), and (c, f) -665 Hz ($r_{IS} = 1.50$ Å) and with values of (a–c) 0 and (d–f) 1978 Hz for $\omega_{CS}^{aniso}/2\pi$. All spectra used $\omega_r/2\pi = \omega_{RF}/2\pi = 6000$ Hz and a Lorentzian line broadening of 135 Hz.
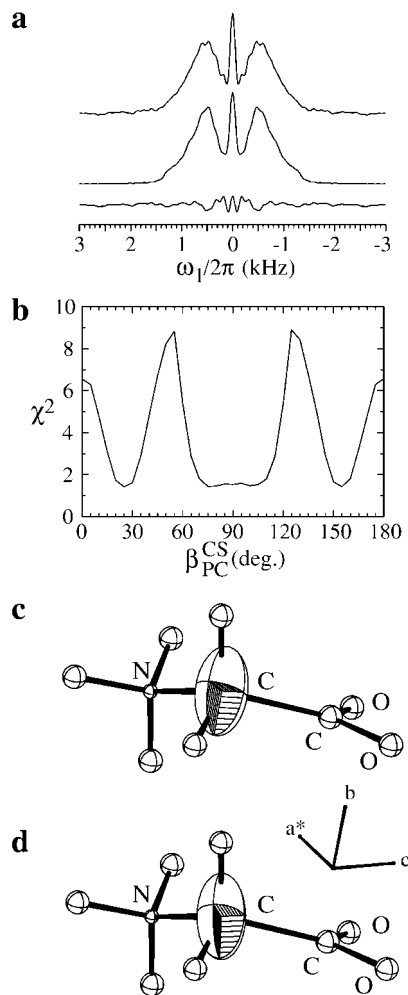
FIG. 6. (a) Experimental and optimum numerically fitted $\omega_1/2\pi$ projections from ^{13}C $n = 1$ 2D rotary resonance ($\omega_r/2\pi = 6000$ Hz) spectra of the ^{13}C$^\alpha$ carbon in glycine along with (b) a χ^2 versus β_{PC}^{CS} scan and ORTEP-like representations of the ^{13}C$^\alpha$ chemical shift tensor as determined (c) in this study for a powder sample and (d) using single-crystal NMR (*37*) (note that γ_{PC}^{CS} is not established from (a) and has been arbitrarily chosen to give the best visual match with (d)). The parameters corresponding to the optimum simulation are given in Table 1, $\omega_{RF}/2\pi = 6178$ Hz, and a Lorentzian line broadening of 136 Hz.

magnitude of the anisotropic interactions. This aspect is addressed in Fig. 5 which, on basis of the L-alanine parameters, illustrates the effect of variations in the dipolar coupling constant between −650, −400, and −150 Hz for the cases with and without ^{13}C chemical shift anisotropy. Finally, we should mention that our analysis did not consider explicitly effects from ^{13}C T_2 and ^{14}N T_1 relaxation. The former may in part explain the 163-Hz linebroadening required for an optimum match between the experimental and simulated spectra, while the latter (which may be in the order of 10 ms according to Weliky and Tycko (*41*)) may lead to partial averaging of the ^{13}C–^{14}N dipolar coupling. The favorable match between the experimental and simulated spectra for L-alanine and glycine

(see below) using a typical one-bond ^{13}C–^{14}N dipolar coupling constant, however, indicates that ^{14}N T_1 relaxation is not a major problem for the samples investigated in this study.

Figure 6 shows the analogous determination of the orientation of the ^{13}C$^\alpha$ chemical shift tensor for glycine achieved by simultaneous recoupling of the anisotropic ^{13}C$^\alpha$ chemical shift and ^{13}C$^\alpha$–^{14}N dipolar coupling interactions using $n = 1$ rotary resonance irradiation on-resonance with respect to ^{13}C$^\alpha$. For glycine the shortest intra- and intermolecular C$^\alpha$–N internuclear distances are 1.509 and 3.87 Å (*35*), corresponding to dipolar coupling constants of −635 and −37.7 Hz, respectively. As for L-alanine, the small intermolecular coupling justifies a two-spin treatment involving the intramolecular ^{13}C$^\alpha$ and ^{14}N spins. Furthermore, the magnitude of the ^{13}C$^\alpha$ chemical shift tensor is known to be $\omega_{CS}^{aniso}/2\pi = 1943$ Hz and $\eta^{CS} = 0.98$ (*37*). From Fig. 6a it is evident that the simulated spectrum obtained through iterative fitting and corresponding to the Euler angles $\alpha_{PC}^{CS} = 79°$ and $\beta_{PC}^{CS} = 26.8°$ agrees very well with the experimental spectrum. By inspection of these Euler angles (see Table 1) and the chemical shift tensors visualized by ORTEP-like plots in Figs. 6c and 6d, it is apparent that the tensor orientation determined in this study for a powder sample with ^{13}C in natural abundance (Fig. 6c) agrees favorably with that earlier established by NMR on an isotope-enriched single crystal of glycine (*37*) (Fig. 6d). We should note that the iterative fitting resulted in two minima with almost the same root-mean-square deviation (the lower one was taken as the optimum solution although ambiguity remains) as illustrated by the χ^2 versus β_{PC}^{CS} scan in Fig. 6b obtained by optimization of the other variables throughout the scan.

From the theoretical description of the rotary resonance experiment, it is clear that the method critically depends on

TABLE 1

Magnitudes and Relative Orientations of ^{13}C$^\alpha$ Chemical Shift and ^{13}C$^\alpha$–^{14}N Dipolar Coupling Tensors Determined for L-Alanine and Glycine Using Natural Abundance ^{13}C $n = 1$ 2D Rotary Resonance NMR on Powder Samples at 9.4 T[a]

	L-Alanine	Glycine
$\omega_{aniso}^{CS}/2\pi$ (Hz)	1978 (*37*)	1943 (*38*)
η^{CS}	0.44 (*37*)	0.98 (*38*)
$b_{IS}/2\pi$ (Hz)	−665 ($r_{IS} = 1.486$ Å (*34*))	−635 ($r_{IS} = 1.509$ Å (*35*))
α_{PC}^{CS} (deg)	−51 ± 30 (−73.1 (*36*))	79 ± 30 (64.9 (*37*))
β_{PC}^{CS} (deg)	21.7 ± 7 (25.5 (*36*))	26.8 ± 10 (37.3 (*37*))
γ_{PC}^{CS} (deg)	116.6[b] (166.4 (*36*))	24.2[b] (−28.8 (*37*))

[a] The Euler angles are given relative to the C$^\alpha$–N bonding axis, i.e., $\Omega_{PC}^{IS} = \{0, 0, 0\}$. Accuracies were estimated using a combination of 95% confidence intervals from χ^2 curves obtained by scanning the relevant parameter while fitting the other variables (see text) and visual inspection of lineshape changes. Numbers with indicated references correspond to previous studies.

[b] γ_{PC}^{CS} can not be determined for isolated ^{13}C–^{14}N spin systems in powder samples. The indicated angles correspond to the ORTEP-like plots in Figs. 3c and 6c.

accurate matching of the RF field strength to the spinning speed according to one of the conditions in Eq. [4]. Consequently, the method is sensitive toward minor mismatch between these two frequencies and toward RF inhomogeneity. Both effects may lead to a reduction in the width of the $\omega_1/2\pi$-dimension powder pattern, which at first sight erroneously may be interpreted in terms of reduced values for the b_{IS} and/or ω_{CS}^{aniso} unless taken explicitly into account in the numerical analysis of the experimental data. Fortunately, these effects are easily identified, as mismatch between ω_{RF} and ω_r causes a longitudinal contribution to the I-spin Hamiltonian in the tilted frame which does not affect the initial operator. Thus, the mismatch will be reflected in a signal at $\omega_1/2\pi = 0$. In case of severe mismatch or large RF inhomogeneities, this resonance and its accompanying sinc wiggles (upon zero-filling) may severely hamper extraction of structural data from the $\omega_1/2\pi$-dimension of the 2D rotary resonance spectra. As a consequence, it is important to calibrate the RF field strengths carefully to obtain the best possible match and ensure that the RF inhomogeneity effects are less than about 5–10%, e.g., by restriction of the sample volume (as in this study) (42) or using coils associated with low RF inhomogeneity (43). Under these circumstances remaining effects from RF inhomogeneity and mismatch may readily be taken into account in the iterative fitting of the experimental spectra. In the present setup the RF homogeneity was sufficiently high that only the rotary resonance match needed to be considered. Through iterative fitting it was established that the spectra in Figs. 3 and 6 ($\omega_r/2\pi = 6000$ Hz) correspond to RF field strengths of 6123 and 6178 Hz, respectively, being required to match all features in the experimental spectra. We note that these values agree very well with the values determined independently from the $\omega_1/2\pi$ splittings observed for the carbonyl carbons in the same rotary resonance spectra for the two compounds under consideration of the actual off-resonance effects. In practice, larger RF inhomogeneities may be handled by measuring the weighted RF field distribution for the carbonyl resonances in the actual spectra (or using an independent nutation experiment (42) for a powder of isolated spin-1/2 nuclei) and including this distribution function in the simulation of the rotary resonance experiment by weighted coaddition of a representative number of spectra calculated using the relevant RF field strengths.

b. Effects from Remote ^{14}N Spins: The ^{14}N–^{13}C–^{14}N Spin System

The absolute orientation of chemical shift tensors relative to the molecular frame may be determined from powder samples, provided that it can be measured in combination with two noncoaxial dipole–dipole coupling tensors. For example, this has been demonstrated recently for ^{13}C–^{13}C–^{14}N (25), $(^{31}$P$)_2$^{113}Cd (44), four-^{13}C (45), and $(^{31}$P$)_2$^{1}H (46) spin systems using MAS NMR with appropriate combination of various re- and decoupling methods. Here we address, as an example, the

backbone carbons in unlabeled peptides, where absolute alignment of the ^{13}C chemical shift tensor to the molecular frame requires resolvable coupling to at least two different ^{14}N nuclei being the only possibility among abundant spin species when disregarding protons. Already at this stage it is emphasized that this "peptide system" only serves as an example of a heteronuclear ^{14}N–^{13}C–^{14}N spin system and that potential difficulties resolving this spin system obviously have to be solved prior to potential practical applications (*vide infra*).

Considering typical internuclear distances, it appears intuitively possible to observe effects from the long-range ^{13}C$_i$–^{14}N$_{i+1}$ dipolar coupling in peptide ^{14}N$_i$–^{13}C$_i$–^{14}N$_{i+1}$ three-spin systems with C_i being C_i^α or C'_i. It is of interest to investigate this aspect in more detail for two reasons. First, if the effect of the long-range coupling is not resolved, the spin-pair approach demonstrated above for unlabeled amino acids in principle applies equally well for unlabeled peptides (provided that the ^{13}C resonances can be resolved and assigned), although still limiting the molecular reference frame for the shift tensor to one axis. Information about the magnitude of the ^{13}C$^\alpha$ (or ^{13}C') chemical shift tensor and its orientation relative to the one-bond ^{13}C–^{14}N axis for peptides may be itself potentially provide important information about the structure of the peptide bond (4, 9–13). Second, if this coupling is manifested sufficiently clearly in the spectra, it should be taken into account in the numerical evaluation and may, as an additional benefit, allow determination of the absolute orientation of the ^{13}C chemical shift tensor.

Since C_i^α shares corners of two adjacent peptide planes, its chemical shift tensor may in a sensitive manner reflect the ϕ_i and ψ_i dihedral angles characterizing the mutual orientation of these peptide planes. Indeed, based on ab initio calculations and experimental data from several tripeptides, Heller *et al.* (9) recently demonstrated that the magnitude of the ^{13}C$^\alpha$ chemical shift tensor is closely related to ϕ and ψ. Further constraints on these angles may very likely be derived from additional information about the absolute or relative orientation of the ^{13}C$^\alpha$ chemical shift tensor (10). To investigate a potential application of the 2D rotary resonance experiment to determine the orientation of ^{13}C$^\alpha$ chemical shift tensors in unlabeled or ^{13}C-labeled peptides, we consider a typical pair of peptide planes, as illustrated in Fig. 7. The distance between C$_i^\alpha$ and the directly attached nitrogen N$_i$ in a specific peptide plane (*i*th amino acid) is 1.53 Å, while the distance to the closest nitrogen N$_{i+1}$ in the adjacent peptide plane ($i + 1$'th amino acid) is 2.40 Å. The latter distance corresponds to a dipolar coupling constant of -157 Hz, being about one quarter of the value for the directly bonded spins but considerably larger than any residual quadrupolar–dipolar coupling cross-term (*vide supra*). Within the ^{14}N$_i$–^{13}C$_i^\alpha$–^{14}N$_{i+1}$ three-spin system the mutual orientation of the N$_i$–C$_i^\alpha$ and C$_i^\alpha$–N$_{i+1}$ internuclear axes (and the corresponding dipolar coupling tensors) depends on the dihedral angle ψ_i, while the orientation of the ^{13}C$_i^\alpha$ chemical shift tensor depends on both dihedral angles ϕ_i and ψ_i. We note that even

for $\psi_i = 0°$ the homonuclear $^{14}N_i-^{14}N_{i+1}$ dipolar coupling is too small to influence the spectra.

Lacking specific knowledge about the relation between the dihedral angles and the absolute orientation of the $^{13}C_i^\alpha$ chemical shift tensor, Fig. 8 shows a series of $\omega_1/2\pi$ sections from $n = 1$ ^{13}C 2D rotary resonance spectra calculated using different orientations of the $^{13}C_i^\alpha$ chemical shift tensor and the $C_i^\alpha-N_{i+1}$ bonding axis relative to the peptide plane containing C_i^α and N_i. These orientations are specified by the Euler angles α_{PC}^{CS}, β_{PC}^{CS}, $\beta_{PC}^{I_iS_{i+1}}$, and $\gamma_{PC}^{I_iS_{i+1}}$ relative to a crystal-fixed frame with z_C parallel to the $N_i-C_i^\alpha$ bonding axis and y_C axis perpendicular to the peptide plane (the principal axis frame of the $^{14}N_i-^{13}C_i^\alpha$ dipolar coupling tensor). While the two former angles are allowed to vary over the full 180° range, the variation of the pair of angles $\{\beta_{PC}^{I_iS_{i+1}}, \gamma_{PC}^{I_iS_{i+1}}\}$ has been restricted to $\{40°, 180°\}$ and $\{100°, 180°\}$, corresponding to the extreme ψ_i angles of 180° and 0°, respectively. Using a 75-Hz Lorentzian line broadening, the spectra display visible dependence on β_{PC}^{CS}, α_{PC}^{CS}, and ψ_i in the given order. We note that the spectra vary smoothly with ψ_i between 0° and 180°, justifying that only the two extremum values are included in the figure. By comparison of the upper and lower rows in Fig. 8 it can be concluded that the spectra display minor effects from the dipolar coupling between $^{13}C_i^\alpha$ and the remote $^{14}N_{i+1}$ spin. These effects are sufficiently large that they should be considered if the method is used to establish orientational information about the $^{13}C_i^\alpha$ chemical shift tensors in peptides, but at the same time too small to render 2D rotary resonance the method of choice for determination of the backbone torsion angles in unlabeled or selectively ^{13}C-labeled peptides.

The $^{13}C'$ chemical shift tensor represents another important source of information about the peptide backbone conformations which may be accessed by ^{13}C rotary resonance NMR. Thus, based on glycine values for the magnitude of $^{13}C'$ chemical shift tensor ($\omega_{CS}^{aniso}/2\pi = -7743$ Hz, $\eta^{CS} = 0.88$) and dipolar coupling constants of $b_{I_iS_{i+1}}/2\pi = -927$ Hz and $b_{I_iS_i}/2\pi = -146$ Hz for a peptide backbone $^{14}N_i-^{13}C_i'-^{14}N_{i+1}$ three-spin system (cf. Fig. 7), Fig. 9 shows a series of simu-

FIG. 8. $\omega_1/2\pi$ projections from ^{13}C $n = 1$ 2D rotary resonance spectra ($\omega_r/2\pi = \omega_{RF}/2\pi = 6000$ Hz) calculated for a peptide backbone $^{14}N_i-^{13}C_i^\alpha-^{14}N_{i+1}$ three-spin system. The calculations assume the same magnitudes for the $^{13}C^\alpha$ chemical shift and $^{13}C_i^\alpha-^{14}N_i$ dipolar coupling tensors as for the $^{13}C^\alpha-^{14}N$ spin pair of glycine (Table 1) and a $^{13}C_i^\alpha-^{14}N_{i+1}$ dipolar coupling constant of -157 Hz (corresponding to $r_{I_iS_{i+1}} = 2.4$ Å). Relative to a molecule-fixed coordinate system with z_C parallel to the $C_i^\alpha-N_i$ axis and y_C perpendicular to the peptide plane containing N_i (cf. Fig. 7), the anisotropic tensors are oriented as $\Omega_{PC}^{I_iS_i} = \{0, 0, 0\}$, $\Omega_{PC}^{CS} = \{\alpha_{PC}^{CS}, \beta_{PC}^{CS}, 0\}$, and $\Omega_{PC}^{I_iS_{i+1}} = \{0, \beta_{PC}^{I_iS_{i+1}}, \gamma_{PC}^{I_iS_{i+1}}\}$. The actual values for α_{PC}^{CS}, β_{PC}^{CS}, and ψ_i are written beside each plot. Using the geometry in Fig. 7 the $\{\beta_{PC}^{I_iS_{i+1}}, \gamma_{PC}^{I_iS_{i+1}}\}$ values of $\{100°, 180°\}$ and $\{40°, 180°\}$ correspond to $\psi_i = 0°$ and 180°, respectively ($\phi_i = 180°$). All spectra were obtained using a Lorentzian line broadening of 75 Hz.

lated rotary resonance spectra for $^{13}C'$ using the same setup as used in Fig. 8. Also in this case the spectra are quite sensitive to the orientation of the $^{13}C'$ chemical shift tensor relative to the $C_i'-N_{i+1}$ internuclear axis. In contrast, with typical line broadening the spectra appear less sensitive to the relatively weak dipolar coupling to the remote $^{14}N_i$ spin, which in turn implies that the sensitivity toward variations in ψ_i is probably too low to be of practical use. The sensitivity of the spectra toward variation in α_{PC}^{CS}, on the other hand, may be of interest to study relations between the peptide backbone structure and the magnitude and orientation of the $^{13}C'$ chemical shift tensor relative to the peptide plane. While the magnitude and orientation (perpendicular to the sp^2 plane) of δ_{zz} appear relatively independent of the residue type and the secondary structure, differences in earlier reported values for the magnitude of δ_{yy} and the orientation of the transverse tensor elements within the peptide plane (*7, 8, 47*) indicate some structural dependency on the ω_{CS}^{aniso}, η^{CS}, and α_{PC}^{CS} parameters that may be interesting to explore for powder samples using the proposed 2D rotary resonance method.

CONCLUSION

In this paper we have demonstrated that the ^{13}C rotary resonance experiment, which simultaneously recouples aniso-
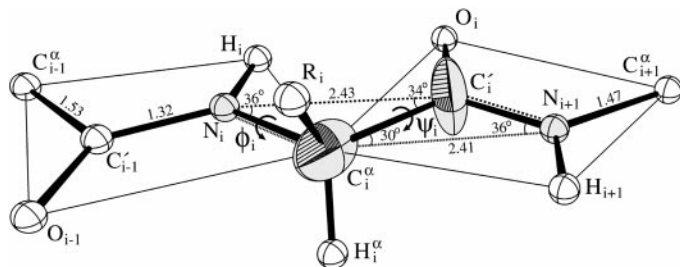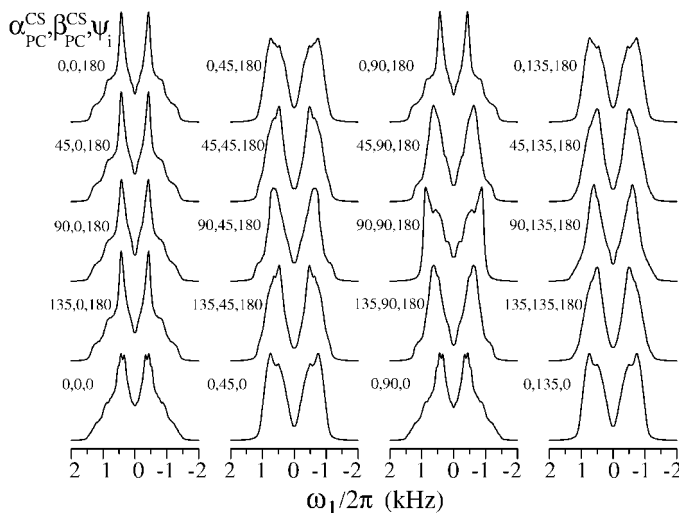

FIG. 7. ORTEP-type representation of two peptide planes defining the dihedral angles ϕ_i and ψ_i, which specify the conformation of the peptide backbone. The plot, using $\phi_i = \psi_i = 180°$, illustrates the two relevant $^{14}N_i-^{13}C_i^\alpha-^{14}N_{i+1}$ and $^{14}N_i-^{13}C_i'-^{14}N_{i+1}$ three-spin systems along with relevant bond angles and the $^{13}C^\alpha$ (arbitrary orientation) and $^{13}C'$ (typical orientation) chemical shift tensors.

$\alpha_{PC}^{CS}, \beta_{PC}^{CS}, \psi_i$

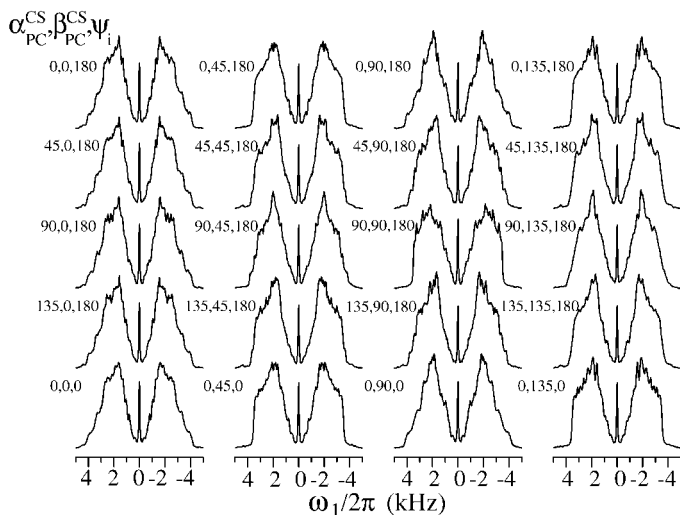**FIG. 9.** $\omega_1/2\pi$ projections from ^{13}C $n = 1$ 2D rotary resonance spectra ($\omega_r/2\pi = \omega_{RF}/2\pi = 6000$ Hz) calculated for a peptide backbone $^{14}N_i-^{13}C'_i-$ $^{14}N_{i+1}$ three-spin system. The calculations assume $\omega_{CS}/2\pi = -7742$ Hz, $\eta^{CS} = 0.88$, $b_{I_iS_{i+1}}/2\pi = -927$ Hz, and $b_{I_iS_i}/2\pi = -146$ Hz. Relative to a molecule fixed coordinate system with z_C parallel to the C'_i-N_{i+1} axis and y_C perpendicular to the peptide plane containing C'_i (cf. Fig. 7), the anisotropic tensors are oriented as $\Omega_{PC}^{I_iS_{i+1}} = \{0, 0, 0\}$, $\Omega_{PC}^{CS} = \{\alpha_{PC}^{CS}, \beta_{PC}^{CS}, 0\}$, and $\Omega_{PC}^{I_iS_i} = \{0, \beta_{PC}^{I_iS_i}, \gamma_{PC}^{I_iS_i}\}$. The actual values for α_{PC}^{CS}, β_{PC}^{CS}, and ψ_i are written beside each plot. $\psi_i = 0°$ and $180°$ correspond to $\{\beta_{PC}^{I_iS_i}, \gamma_{PC}^{I_iS_i}\}$ values of $\{80°, 180°\}$ and $\{148°, 180°\}$, respectively ($\phi_i = 180°$). All spectra were obtained using a Lorentzian line broadening of 75 Hz.

tropic effects from ^{13}C chemical shift and $^{13}C-^{14}N$ dipolar coupling tensors in $^{13}C-^{14}N$ and $^{14}N-^{13}C-^{14}N$ spin systems, represents a feasible approach to obtain information about the magnitude and orientation of ^{13}C chemical shift tensors for powder samples. For example, the method may find applications for determination of the orientation of the ^{13}C chemical shielding tensor relative to the one-bond $^{13}C-^{14}N$ internuclear axis in unlabeled or selectively ^{13}C-labeled amino acids and small peptides. The method may also find interesting applications for other types of spin-1/2 to spin-1 coupled spin systems such as $^{13}C-^{2}H$ or $^{29}Si-^{14}N$ in inorganic systems. As a particularly attractive feature, the method does not rely on irradiation of the quadrupolar nuclei, implying that the triple-resonance effects may be observed on standard double-resonance solid-state NMR instrumentation.

ACKNOWLEDGMENTS

REFERENCES

1. N. Tjandra and A. Bax, Direct measurement of distances and angles in biomolecules by NMR in a dilute liquid crystalline medium, *Science* **278**, 1111–1114 (1997).

2. J. H. Prestegard, New techniques in structural NMR—Anisotropic interactions, *Nat. Struct. Biol.* **5**, 517–522 (1998).

3. M. R. Hansen, L. Mueller, and A. Pardi, Tunable alignment of macromolecules by filamentous phage yields dipolar coupling interactions, *Nat. Struct. Biol.* **5**, 1065–1074 (1998).

4. C. D. Kroenke, M. Rance, and A. G. Palmer, Variability of ^{15}N chemical shift anisotropy in *Escherichia coli* ribonuclease H in solution, *J. Am. Chem. Soc.* **121**, 10119–10125 (1999).

5. R. G. Griffin, Dipolar recoupling in MAS spectra of biological solids, *Nat. Struct. Biol.* **5**, 508–512 (1998).

6. X. Feng, M. Edén, A. Brinkmann, H. Luthman, L. Erikson, A. Gräslund, O. N. Antzutkin, and M. H. Levitt, Direct determination of a peptide torsional angle ψ by double-quantum solid-state NMR, *J. Am. Chem. Soc.* **119**, 12006–12007 (1997).

7. H. W. Long and R. Tycko, Biopolymer conformational distribution from solid-state NMR: α-Helix and 3_{10}-helix contents of a helical peptide, *J. Am. Chem. Soc.* **120**, 7039–7048 (1998).

8. K. Nomura, K. Takegoshi, T. Terao, K. Uchida, and M. Kainosho, Determination of the complete structure of a uniformly labeled molecule by rotational resonance solid-state NMR in the tilted rotating frame, *J. Am. Chem. Soc.* **121**, 4064–4065 (1999).

9. J. Heller, D. D. Laws, M. Tomaselli, D. S. King, D. E. Wemmer, A. Pines, R. H. Havlin, and E. Oldfield, Determination of dihedral angles in peptides through experimental and theoretical studies of alpha-carbon chemical shielding tensors, *J. Am. Chem. Soc.* **119**, 7827–7831 (1997).

10. R. H. Havlin, H. Le, D. D. Laws, A. C. deDios, and E. Oldfield, An ab initio quantum chemical investigation of carbon-13 NMR shielding tensors in glycine, alanine, valine, isoleucine, serine, and threonine: Comparisons between helical and sheet tensors, and the effect of χ_1 on shielding, *J. Am. Chem. Soc.* **119**, 11951–11958 (1997).

11. C. Scheurer, N. R. Skrynnikov, S. F. Lienin, S. K. Straus, R. Brüschweiler, and R. R. Ernst, Effects of dynamics and environment on ^{15}N chemical shielding anisotropy in proteins. A combination of density functional theory, molecular dynamics simulation, and NMR relaxation, *J. Am. Chem. Soc.* **121**, 4242–4251 (1999).

12. Y. Wei, A. deDios, and A. E. McDermott, Solid-State ^{15}N NMR chemical shift anisotropy of histidine: Experimental and theoretical studies of hydrogen bonding, *J. Am. Chem. Soc.* **121**, 10389–10394 (1999).

13. D. K. Lee, R. J. Wittebort, and A. Ramamoorthy, Characterization of ^{15}N chemical shift and $^1H-^{15}N$ dipolar coupling interactions in a peptide bond of uniaxially oriented and polycrystalline samples by one-dimensional dipolar chemical shift solid-state NMR, *J. Am. Chem. Soc.* **120**, 8868–8874 (1998).

14. D. P. Raleigh, M. H. Levitt, and R. G. Griffin, Rotational resonance in solid state NMR, *Chem. Phys. Lett.* **146**, 71–76 (1988).

15. T. G. Oas, R. G. Griffin, and M. H. Levitt, Rotary resonance recoupling of dipolar interactions in solid-state nuclear magnetic resonance spectroscopy, *J. Chem. Phys.* **89**, 692–695 (1988).

16. M. H. Levitt, T. G. Oas, and R. G. Griffin, Rotary resonance recoupling in heteronuclear spin pair systems, *Isr. J. Chem.* **28**, 271–282 (1988).

17. T. Gullion and J. Schaefer, Rotational-echo double-resonance NMR, *J. Magn. Reson.* **81**, 196–200 (1989).

18. A. E. Bennett, J. H. Ok, R. G. Griffin, and S. Vega, Chemical shift correlation spectroscopy in rotating solids: Radio frequency-driven dipolar recoupling and longitudinal exchange, *J. Chem. Phys.* **96**, 8624–8627 (1992).

19. N. C. Nielsen, H. Bildsøe, H. J. Jakobsen, and M. H. Levitt, Double-quantum homonuclear rotary resonance: Efficient dipolar recovery

in magic-angle spinning nuclear magnetic resonance, *J. Chem. Phys.* **101,** 1805–1812 (1994).

20. M. Baldus, M. Tomasselli, B. H. Meier, and R. R. Ernst, Broadband polarization-transfer experiments for rotating solids, *Chem. Phys. Lett.* **230,** 329–336 (1994).

21. D. M. Gregory, D. J. Mitchell, J. A. Stringer, S. Kiihne, J. C. Shiels, J. Callahan, M. A. Mehta, and G. P. Drobny, Windowless dipolar recoupling: The detection of weak dipolar interactions between spin 1/2 nuclei with large chemical shift anisotropies, *Chem. Phys. Lett.* **246,** 654–663 (1995).

22. Y. K. Lee, N. D. Kurur, M. Helmle, O. G. Johannessen, N. C. Nielsen, and M. H. Levitt, Efficient dipolar recoupling in the NMR of rotating solids. A sevenfold symmetric radiofrequency pulse sequence, *Chem. Phys. Lett.* **242,** 304–309 (1995).

23. M. Hohwy, H. J. Jakobsen, M. Edén, M. H. Levitt, and N. C. Nielsen, Broadband dipolar recoupling in the nuclear magnetic resonance of rotating solids: A compensated C7 pulse sequence, *J. Chem. Phys.* **108,** 2686–2694 (1998).

24. Z. Gan, D. M. Grant, and R. R. Ernst, NMR chemical shift anisotropy measurements by RF driven rotary resonance, *Chem. Phys. Lett.* **254,** 349–357 (1996).

25. M. Bak and N. C. Nielsen, Relative orientation of chemical shielding and dipolar coupling tensors: Mixed single- and double-quantum homonuclear rotary resonance nuclear magnetic resonance of rotating solids, *J. Chem. Phys.* **106,** 7587–7599 (1997).

26. J. G. Hexem, M. H. Frey, and S. J. Opella, Molecular and structural information from ^{14}N–^{13}C dipolar couplings manifested in high-resolution ^{13}C NMR spectra of solids, *J. Chem. Phys.* **77,** 3847–3856 (1982).

27. A. C. Oliviery, L. Frydman, and L. E. Diaz, A simple approach for relating molecular and structural information to the dipolar coupling ^{13}C–^{14}N in CPMAS NMR, *J. Magn. Reson.* **75,** 50–62 (1987).

28. Z. Gan and D. M. Grant, Molecular and structural information from variable-angle spinning NMR dipolar spectra of ^{13}C–^{14}N systems, *J. Magn. Reson.* **90,** 522–534 (1990).

29. C. P. Grey, W. S. Veeman, and A. J. Vega, Rotational echo ^{14}N/^{13}C/^{1}H triple resonance solid-state nuclear magnetic resonance: A probe of ^{13}C–^{14}N internuclear distances, *J. Chem. Phys.* **98,** 7711–7724 (1993).

30. I. Sack, A. Goldbourt, S. Vega, and G. Buntkowsky, Deuterium REDOR: Principles and applications for distance measurements, *J. Magn. Reson.* **138,** 54–65 (1999).

31. T. Gullion, A comparison between REDOR and θ-REDOR for measuring ^{13}C–^{2}D dipolar interactions in solids, *J. Magn. Reson.* **139,** 402–407 (1999).

32. D. Sandström, M. Hong, and K. Schmidt-Rohr, Identification and mobility of deuterated residues in peptides and proteins by ^{2}H–^{13}C solid-state NMR, *Chem. Phys. Lett.* **300,** 213–220 (1999).

33. A. Naito, S. Ganapathy, and C. A. McDowell, High-resolution solid state ^{13}C NMR spectra of carbons bound to nitrogen in a sample spinning at the magic angle, *J. Chem. Phys.* **74,** 5393–5397 (1981).

34. M. S. Lehmann, T. F. Koetzle, and W. C. Hamilton, Precision neutron diffraction structure determination of protein and nucleic acid components I. The crystal and molecular structure of the amino acid L-alanine, *J. Am. Chem. Soc.* **94,** 2657–2660 (1972).

35. P. G. Jönsson and Å. Kvick, Precision neutron diffraction structure determination of protein and nucleic acid components III. The crystal and molecular structure of the amino acid α-glycine, *Acta Crystallogr.* **B28,** 1827–1833 (1972).

36. A. Naito, S. Ganapathy, K. Akasaka, and C. A. McDowell, Chemical shielding tensor and ^{13}C–^{14}N dipolar splitting in single crystals of L-alanine, *J. Chem. Phys.* **74,** 3190–3197 (1981).

37. R. A. Haberkorn, R. E. Stark, H. van Willigen, and R. G. Griffin, Determination of bond distances and bond angles by solid-state nuclear magnetic resonance. ^{13}C and ^{14}N NMR study of glycine, *J. Am. Chem. Soc.* **103,** 2534–2539 (1981).

38. M. Bak, J. T. Rasmussen, and N. C. Nielsen, SIMPSON: A general simulation program for solid-state NMR spectroscopy, *J. Magn. Reson.* **147,** 296–330 (2000). Web-address and download site for the SIMPSON program: http://nmr.imsb.au.dk.

39. M. Bak and N. C. Nielsen, REPULSION, a novel approach to efficient powder averaging in solid-state NMR, *J. Magn. Reson.* **125,** 132–139 (1997).

40. M. Hohwy, H. Bildsøe, H. J. Jakobsen, and N. C. Nielsen, Efficient spectral simulations in NMR of rotating solids. The γ-COMPUTE algorithm, *J. Magn. Reson.* **136,** 6–14 (1999).

41. D. P. Weliky and R. Tycko, Determination of peptide conformations by two-dimensional magic angle spinning NMR exchange spectroscopy with rotor synchronization, *J. Am. Chem. Soc.* **118,** 8487–8488 (1996).

42. N. C. Nielsen, H. Bildsøe, and H. J. Jakobsen, RF field inhomogeneity in a MAS probe evaluated by MAS nutation NMR of quadrupolar nuclei, *J. Magn. Reson.* **98,** 665–673 (1992).

43. F. H. Larsen, P. Daugaard, H. J. Jakobsen, and N. C. Nielsen, Improving RF field homogeneity in solid-state MAS NMR using a loop-gap resonator, *J. Magn. Reson. A* **115,** 283–286 (1995).

44. S. Dusold and A. Sebald, Magnitudes and orientations of NMR interaction tensors in isolated three-spin systems ABX, *Mol. Phys.* **95,** 1237–1245 (1998).

45. S. Dusold, H. Maisel, and A. Sebald, Magnitudes and orientations of interaction tensors determined from rotational resonance MAS NMR lineshapes of a four-^{13}C-spin system, *J. Magn. Reson.* **141,** 78–90 (1999).

46. J. T. Rasmussen, M. Hohwy, H. J. Jakobsen, and N. C. Nielsen, Magnitude and absolute orientation of ^{1}H chemical shielding tensors in polycrystalline powders: A ^{1}H CRAMPS NMR study of KH$_2$PO$_4$, *Chem. Phys. Lett.* **314,** 239–245 (1999).

47. T. G. Oas, C. J. Hartzell, T. J. McHanon, G. Drobny, and F. W. Dahlquist, The carbonyl ^{13}C chemical shift tensors of five peptides determined from ^{15}N dipole-coupled chemical shift powder patterns, *J. Am. Chem. Soc.* **109,** 5956–5962 (1987).